PAPER

Check for updates

Quantitative activity–activity relationship (QAAR) driven design to develop hydroxamate derivatives of pentanoic acids as selective HDAC8 inhibitors: synthesis, biological evaluation and binding mode of interaction studies†

Sk. Abdul Amin, [ID] [a] Prakruti Trivedi,[b] Nilanjan Adhikari, [ID] [a] Ganesh Routholla,[b] Dhanya Vijayasarathi,[b] Sanjib Das,[a] Balaram Ghosh [ID] *[b] and Tarun Jha [ID] *[a]

Histone deacetylase 8 (HDAC8) has been implicated as a potential drug target of many diseases including cancer. HDAC8 isoform selectivity over other class-I HDACs is a major concern nowadays. In this work, a series of pentanoic acid based hydroxamates with different substituted cap groups have been designed, synthesized, characterized, and screened against class-I HDACs. A quantitative activity–activity relationship (QAAR) model was developed to design HDAC8 selective inhibitors. The designed compounds obtained through the molecular modeling study were synthesized, characterized, and their enzymatic as well as cytotoxic activities were measured. Two compounds **7i** and **7f** are found to be selective HDAC8 inhibitors over other class-I HDACs. These compounds possess better antiproliferative activities against some cancer cell lines. These observations are in agreement with the molecular docking studies for the binding mode of interactions. Further studies show that compounds **7i** and **7f** induce significant cell growth arrest in the G2/M phase, indicating their anticancer potentials. In summary, our study confirms pentanoic acid based hydroxamate as selective HDAC8 inhibitors and two compounds **7i** and **7f** may serve as lead molecules for further investigation.

Introduction

Epigenetic regulation of genes *via* post-translational modulation in proteins results in a heritable change in gene function that culminates in a phenotypic change without altering DNA sequences. Epigenetics plays important roles in cellular and molecular regulatory processes.[1–3] It is associated with DNA methylation, histone modification, chromatin structural remodeling, and noncoding RNA regulation. Among these, histone acetylation and deacetylation are widely occurring post-translational modification processes. Histone deacetylases (HDACs) constitute about 23% of the total domain of epigenetic targets after methyltransferases.[2] These are mainly responsible for balancing the acetylation/deacetylation of lysine amino acids

on histone/nonhistone proteins along with histone acetyltransferase (HAT).[3]

The aberrant expression of various HDACs has been observed in many human diseases, especially in cancer, which makes them important therapeutic targets for many human cancers.[4,5] Overexpression of classical HDACs has been represented in the pathological situation. Hence, histone deacetylase inhibitors (HDACIs) have emerged as promising cancer therapeutic agents.[6]

Zinc dependent HDACs are divided into three main classes: class-I HDACs (HDAC1, 2, 3, 8), class-II consists of class-IIa HDACs (HDAC4, 5, 7, 9) and class-IIb HDACs (HDAC6, 10), class-IV HDAC (HDAC11).[7] The class-III HDACs are called sirtuins and depend on nicotinamide adenine dinucleotide (NAD). These have different mechanism from classical zinc dependent HDACs.[7] HDAC8, a class I HDAC enzyme, is expressed in various tissues and involved in the genesis of malignancy. HDAC8 is localized in the nucleus and expressed ubiquitously (cytogenetic location: Xq 13.1). It also alters epigenetic modification.[6] HDAC8 pivotally controls cellular processes, such as muscle contraction, energy homeostasis, and separation of sister chromatid.[3,5] It is one of the essentials

[a] *Natural Science Laboratory, Division of Medicinal and Pharmaceutical Chemistry, Department of Pharmaceutical Technology, Jadavpur University, Kolkata 700032, India. E-mail: tjupharm@yahoo.com*

[b] *Epigenetic Research Laboratory, Department of Pharmacy, BITS-Pilani, Hyderabad Campus, Shamirpet, Hyderabad 500078, India. E-mail: balaram@hyderabad.bits-pilani.ac.in*

† Electronic supplementary information (ESI) available. See DOI: 10.1039/d1nj02636d
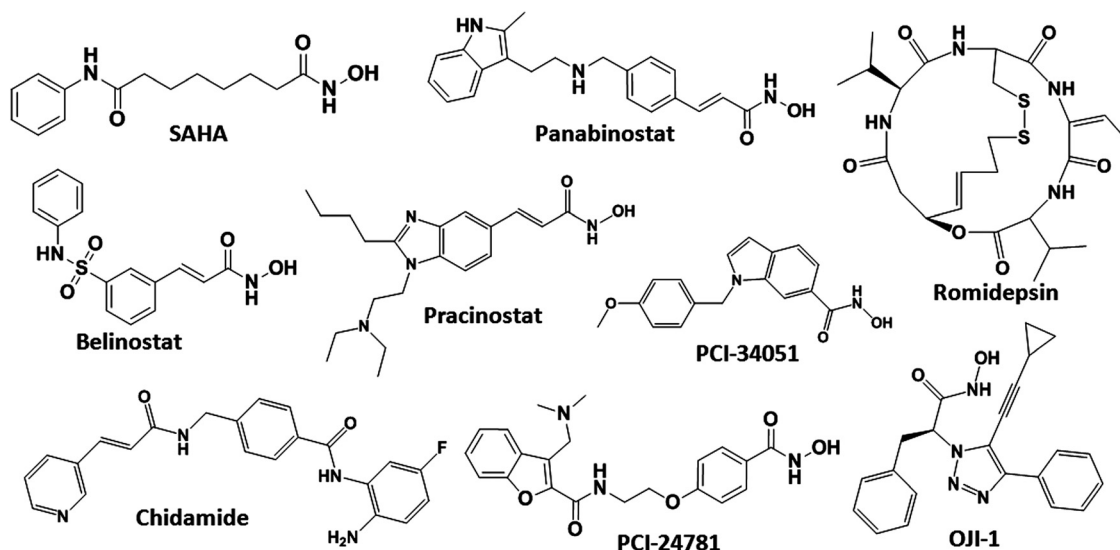
Fig. 1   Structure of hydroxamic acid containing HDAC inhibitors, which are used in clinics or in clinical trials.

for cell survival, and it is implicated in the recently described Cornelia de Lange syndrome (CdLS), which is a congenital malformation disorder.[6] It plays an important role in some diseases, including smooth muscle cell contractions, acute myeloid leukemia, neuroblastoma, and T cell leukemia.[8]

Recently, HDAC8 is emerged as an anticancer target to design molecules against a variety of haematological malignancies.[3] However, target specific HDAC8 inhibitor is still a challenge to medicinal chemists. Many of the HDAC inhibitors currently in the clinics are broad-spectrum or pan-HDAC inhibitors (mainly hydroxamates), which inhibit many of the class I, II, and IV isoforms (Fig. 1).

Among these compounds, vorinostat/SAHA, panobinostat/LBH589, romidepsin/FK228, belinostat/PXD101, and pracinostat/SB939 have been approved by the US-FDA, whereas chidamide/CS055/HBI-8000 is approved by the China Food and Drug Administration (Fig. 1).[3] These compounds have been shown to inhibit most of the HDAC isoforms with nanomolar potency; interestingly, the isoform that is inhibited least potently in each case is the Class I isoform. However, most of these pan-HDACIs failed to pass the Phase II clinical trials due to unwanted adverse effects. Despite these failures, studies on identifying effective and selective HDAC8 inhibitors are still going on.

Drug discovery is a time-consuming process, which requires huge money and manpower.[9,10] To meet this challenge, quantitative structure–activity relationship (QSAR) methods for correlating the physicochemical properties with desired target endpoint are a good initiative.[11,12] Herein, the application of computationally inexpensive chemical descriptors in combination with robust supervised statistical and machine learning approaches was demonstrated for the development of QSAR models.

To achieve the goal to find selective HDAC8 inhibitors, here, we cover six aspects – (i) development of statistically robust quantitative activity–activity relationship (QAAR) model to design new compounds, (ii) synthesis and characterization of a series of designed compounds having aliphatic side chain as a linker with a hanging aliphatic moiety between the ZBG and cap region, (iii) screening for HDAC inhibition potency and selectivity, (iv) cytotoxicity evaluation and understanding of the structure–activity relationships (SARs), (v) cell cycle analysis of two promising compounds, and (vi) possible binding mode of interactions of promising compounds in the drug-binding pockets of the HDAC8 enzyme. This was done to see whether we are getting possible lead molecules or not against murine melanoma, non-small cell lung carcinoma (NSCLC), and acute lymphoblastic leukemia (ALL). This work is a part of our quest of anticancer drug development[4,8,13–16] and surely enriches the research community to find better active agents in the future.

Results and discussion

The present investigation employs QAAR models to design the selective HDAC8 inhibitors that reliably correlated the biological data.

Design of molecules: quantitative activity–activity relationship (QAAR) studies

In order to design selective HDAC8 inhibitors, regression analysis based models were developed and validated. These predictive and validated models were utilized to understand the structural requirements of selective HDAC8 inhibitors and to predict the activity of the designed molecules.

The dataset containing fifty-nine diverse molecules having HDAC8 and HDAC3 inhibitory activities was collected from the published work of the University of Illinois at Chicago[17–26] to perform the QAAR studies (Table S1 of the ESI†). The 2D structures of investigated compounds were drawn by ChemDraw Ultra 8.0 software[27] followed by geometry optimizations. Then, the 2D descriptors were calculated by "PaDEL-descriptor".[28] Finally, multivariate regression analyses were performed to correlate the

Table 1 Contributions of descriptors of eqn (1)

Descriptor	Definition	Contribution
nAtomLAC	Number of atoms in the longest aliphatic chain	Negative
PubchemFP357	C($\sim$C)(:C)(:N)	Negative
PubchemFP300	N–N	Positive
PubchemFP2	$\geq$16 H; hierarchic element counts – these bits test for the presence or count of individual chemical atoms represented by their atomic symbol.	Negative
GATS6v	Geary autocorrelation of lag 6 weighted by van der Waals volume	Positive
PubchemFP528	[#1]–N–C–[#1]	Positive
GATS3s	Geary autocorrelation of lag 3 weighted by I-state	Positive
PubchemFP713	Cc1ccc(C)cc1	Positive

independent descriptors, which in our case are the "PaDEL-descriptors" with the dependent variable (pIC$_{50}^{\text{HDAC8/HDAC3}}$).[29,30] The predictability of the developed model was evaluated using both internal and external validation matrices.[11,31–33]

Lastly, the statistically robust QAAR model was obtained using a linear technique, which is mentioned below:

$$pIC_{50}^{(\text{HDAC8/HDAC3})} = -4.471\,(\pm1.966) - 0.435\,(\pm0.065)\,nAtomLAC$$
$$- 2.322\,(\pm0.176)\,PubchemFP357 + 2.261\,(\pm0.282)$$
$$PubchemFP300 - 4.118\,(\pm0.441)\,PubchemFP2 + 7.587\,(\pm1.716)$$
$$GATS6v + 1.724\,(\pm0.301)\,PubchemFP528 + 2.831\,(\pm0.888)$$
$$GATS3s + 0.797\,(\pm0.313)\,PubchemFP713 \qquad (1)$$

$N_{\text{Train}} = 45$; $R = 0.978$; $R^2 = 0.956$; $R_{\text{A}}^2 = 0.946$; SEE = 0.408; $F_{(8,36)} = 96.720$; $p < 0.00$; $Q^2 = 0.932$; average $r_{\text{m(LOO)}}^2 = 0.904$; $\Delta r_{\text{m(LOO)}}^2 = 0.030$; $N_{\text{Test}} = 14$; $R_{\text{Test}}^2 = 0.971$; $R_{\text{Pred}}^2 = 0.954$; average $r_{\text{m(Test)}}^2 = 0.880$; $\Delta r_{\text{m(Test)}}^2 = 0.028$.

Eqn (1) corresponds to the best QAAR model achieved using the S-MLR technique. The descriptors (Table 1) in this model help to explore the structural requirements to attain HDAC8 selectivity over HDAC3.

The internal parameters, such as $R^2 = 0.956$; $Q^2_{(\text{LOO})} = 0.932$; average $r^2_{\text{m(LOO)}} = 0.904$; $\Delta r^2_{\text{m(LOO)}} = 0.030$, indicate the better predictive potential of the developed QAAR model. Correlation matrix, t-values, and p-values of eqn (1) are shown in the ESI,† Tables S2 and S3 respectively. The Y randomization results (average $R = 0.426$; average $R^2 = 0.195$; average $Q^2_{(\text{LOO})} = -0.397$; $cR^2_{\text{p}} = 0.865$) further confirm the robustness of the QAAR

model. R^2 and Q^2 values after several Y-randomization tests for eqn (1) are shown in ESI† (Table S4).

Euclidean distance-based applicability domain suggests that all the training and test set compounds are within the boundary of this hypothetical domain, as depicted in Fig. 2.

Hence, no outlier is found for this dataset.

The nAtomLAC is a 2D descriptor showing the negative contribution to the HDAC8 selectivity. It defined the total number of atoms in the longest aliphatic chain. The GATS6v, a 2D autocorrelation descriptor, signifies the Geary autocorrelation of lag 6 weighted by van der Waals volume. It shows the positive contribution to the selectivity, which indicates that molecules with higher van der Waals volume will show higher selectivity. Another 2D autocorrelation descriptor, GATS3s defines Geary autocorrelation of lag 3 weighted by I-state. This descriptor has a positive contribution to the HDAC8 selectivity over HDAC3. It carries information concerning the topology of an atom and the electronic interactions due to all other atoms in the molecule. The bond orders and bond aromaticity are also found to be important. Lastly, to design the HDAC8 selective inhibitors, these favorable fingerprints were taken into consideration so that the specificity to HDAC8 may be ensured.

Similarly, support vector machine (SVM) regression analysis was performed on the training set (45 compounds) using the same descriptors. Likewise, a search for the parameters tuning was carried out in a stepwise manner. The SVM parameters (The complexity parameter $C = 1.0$, exponent $E = 1.0$, epsilon parameter = 0.001, tolerance $T = 0.001$) were used to construct the SVM model. Here, we used John Platt's Sequential Minimal Optimization (SMO) algorithm with the Waikato Environment for Knowledge Analysis (Weka) version 3.8.4.[34,35] The predictive performance derived from SVM as well as MLR models are shown in Table 2.
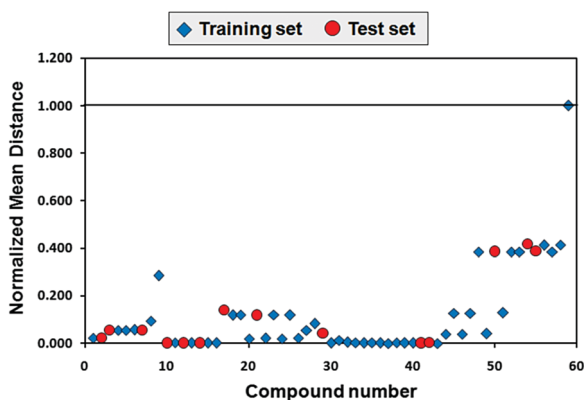

Fig. 2 Graphical representation of applicability domain of eqn (1) by the Euclidean distance approach.

Table 2 Predictive performance of MLR and SVM models using the training and test data sets

Parameter	MLR			SVM		
	r	MAE	RMSE	r	MAE	RMSE
Train set	0.978	0.277	0.365	0.974	0.269	0.413
Test set	0.985	0.279	0.316	0.984	0.249	0.276

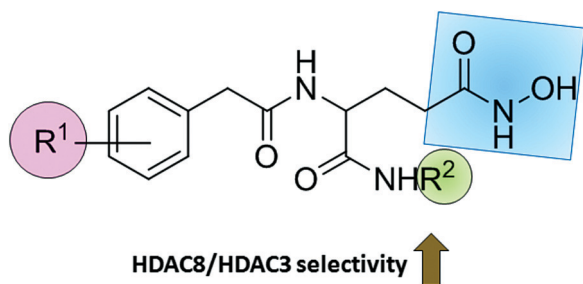r, correlation coefficient; MAE, mean absolute error; RMSE, root mean square error.

Fig. 3 General structure of the designed inhibitors.

Results indicated that SVM regression analysis (r = 0.974, MAE = 0.269 and RMSE = 0.413) performed similarly with the S-MLR approach (r = 0.978, MAE = 0.277 and RMSE = 0.365). Further evaluation of the predictive performance of the QAAR model on the training data set was performed using the same data sampling approaches, including 5-fold cross-validation (S-MLR model: r_{5CV} = 0.967; SVM model: r_{5CV} = 0.964) and 10-fold cross-validation (S-MLR model: r_{10CV} = 0.958; SVM model: r_{10CV} = 0.951). Interestingly, all cross-validation methods achieved good performances. Of the two multivariate regression methods used in this study, SVM analysis was found to be similar to the traditional regression methods such as S-MLR. Hence, it may be postulated that the use of these molecular descriptors yield good predictive performances.

For this study, we concentrated on the 2D descriptor, *nAtomLAC*. This descriptor suggests that the presence of more number of atoms in the longest aliphatic chain contributes negatively to the HDAC8 selectivity over HDAC3. It has been reported in the literature that class I enzymes have an internal pocket at the bottom of the tube-like channel leading to the zinc ion.[4] This 14 Å hydrophobic internal cavity is formed by the same residues for all class I isoforms with minor differences. HDAC1, HDAC2, and HDAC3 in that order contain the longest cavities, and HDAC-8 has the smallest one.[36] Recent reports reveal that HDAC8 possesses a deep hydrophobic pocket adjacent to the active site channel allowing the design of HDAC8 selective compounds that interact with both the active site Zn^{2+} ion and this sub pocket. These unique features can be exploited to design selective compounds for class I HDACs.[10] Now, it is clear that these compounds have short length of linker moiety as well as side chains attached to the linker improve the biological activity.[11]

From the results of QAAR studies, the understanding of SAR of this series of compounds of the dataset becomes clearer and specific conclusions can be made. Also, the reported QAAR models pass all the requisite validation criteria. Hence, they are useful for predicting the activity/selectivity of a similar class of compounds.

The information obtained in the QAAR model was analyzed to design compounds, which were predicted to show the selectivity towards HDAC8. A series of compounds having an aliphatic side chain as a linker with a hanging aliphatic moiety between the ZBG and cap region has been designed. Depending on our earlier observations[3,4,8] as well as observation from the current QAAR study, these compounds are designed. The general structure of the designed inhibitors is depicted in Fig. 3.

Most of the designed compounds were predicted as 'selective' HDAC8 inhibitors in these regression models, as shown in Table 3. The values of descriptors and the predicted activity ranges are given in the ESI† (Table S5).

After the design of molecules, we turned our attention to validate the QAAR models experimentally. In this connection, we synthesised the designed compounds, and subsequently, the purity of compounds was evaluated using ^{1}H NMR, ^{13}C NMR, and LC/MS analyses.

Chemistry

A series of compounds having an aliphatic side chain as a linker with a hanging aliphatic moiety between the ZBG and cap region have been synthesized (Scheme 1).

The purity of these final compounds was evaluated using ^{1}H NMR, ^{13}C NMR, and LC/MS analyses. Spectral data of these compounds are provided below:

Table 3 Designed molecules with their predicted HDAC8/HDAC3 selectivity

Comp[a]	R^1	R^2	Predicted HDAC8/HDAC3 selectivity		Average predicted HDAC8/HDAC3 selectivity[b]	Predicted HDAC8/HDAC3 selectivity range		Average Predicted HDAC8/HDAC3 selectivity range
			MLR	SVM		MLR	SVM	
7a	2-Br	n-C$_5$H$_{11}$	1.035	0.168	0.602	SEL	SEL	SEL
7b	2-F	i-C$_4$H$_9$	0.934	0.885	0.910	SEL	SEL	SEL
7c	4-Br	n-C$_5$H$_{11}$	0.912	0.355	0.634	SEL	SEL	SEL
7d	4-Br	n-C$_6$H$_{13}$	0.654	0.035	0.345	SEL	SEL	SEL
7e	4-Cl	n-C$_4$H$_9$	0.628	0.693	0.661	SEL	SEL	SEL
7f	4-Cl	n-C$_5$H$_{11}$	0.564	0.383	0.474	SEL	SEL	SEL
7g	4-NO$_2$	n-C$_4$H$_9$	0.448	0.425	0.437	SEL	SEL	SEL
7h	2,4-Dichloro	n-C$_4$H$_9$	0.232	0.629	0.431	SEL	SEL	SEL
7i	2,4-Dichloro	n-C$_5$H$_{11}$	0.195	0.320	0.258	SEL	SEL	SEL
7j	2,4-Dichloro	C$_6$H$_5$	0.143	0.921	0.532	SEL	SEL	SEL
7k	—	n-C$_5$H$_{11}$	−0.074	1.267	0.597	NS	SEL	SEL
7l	—	n-C$_6$H$_{13}$	−0.208	0.945	0.369	NS	SEL	SEL

[a] Compound number. [b] Average predicted selectivity [(MLR + SVM)/2] as per the QAAR models; SEL, HDAC8 selective (positive value); NS, non-selective (negative value).
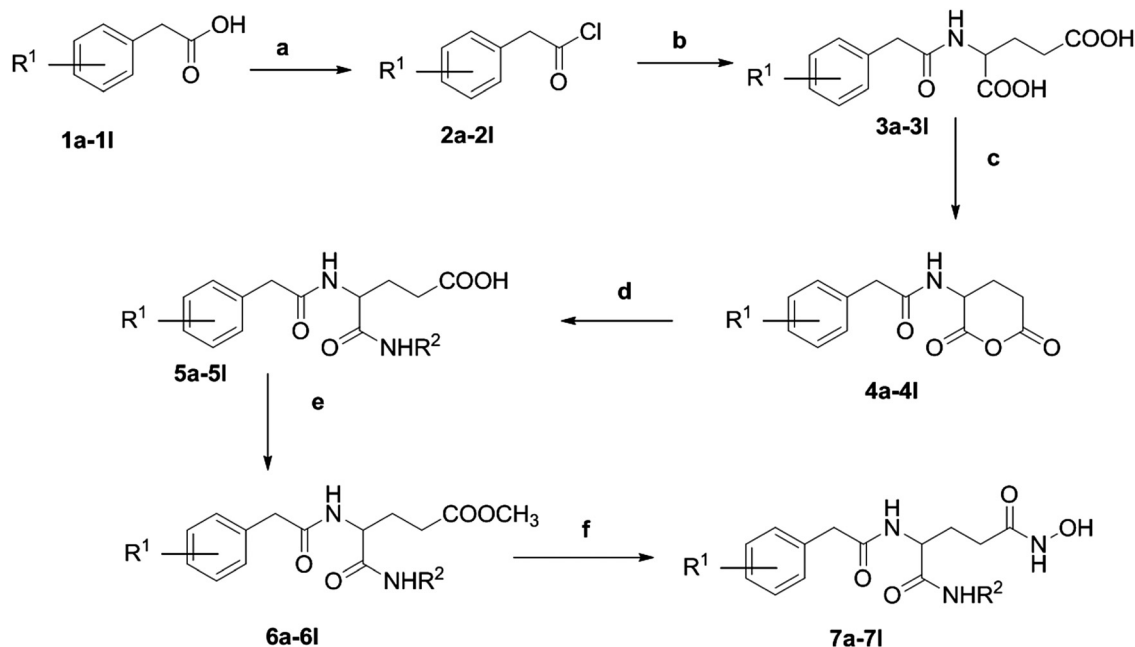
Scheme 1 Reagents & conditions: (a) (i) thionyl chloride (ii) benzene (b) (i) L(+) glutamic acid (ii) 2 N NaOH (iii) 1 N HCl (c) (i) DCC (ii) Chloroform (d) (i) R_2NH_2 (ii) 1 N Na_2CO_3 (iii) 1 N HCl (e) (i) thionyl chloride, (ii) anhydrous methanol, 12 h, 0 °C (f) (i) 50% w/v aqueous hydroxylamine solution, (ii) 1 N sodium hydroxide, (iii) methanol (1 : 1), 2 h, RT (iv) 1 M hydrochloric acid.

2-(2-(2-Bromophenyl) acetamido)-N^5-hydroxy-N^1-pentylpentanediamide (7a). Yield 56.09%, white solid, ^{1}H NMR (400 MHz, DMSO-d_6) δ 10.42 (s, 1H), 8.25 (d, J = 8.1 Hz, 1H), 7.90 (t, J = 5.4 Hz, 1H), 7.58 (d, J = 7.9 Hz, 1H), 7.32 (q, J = 7.5 Hz, 2H), 7.21–7.15 (m, 1H), 4.22 (dd, J = 13.7, 8.0 Hz, 1H), 3.71–3.60 (m, 2H), 3.11–2.97 (m, 2H), 2.06–1.67 (m, 4H), 1.43–1.16 (m, 7H), 0.85 (t, J = 6.9 Hz, 3H), ^{13}C NMR (101 MHz, DMSO-d_6) δ 170.73, 168.77, 168.50, 136.03, 132.18, 131.80, 128.54, 127.49, 124.45, 52.34, 42.10, 38.39, 28.86, 28.65, 28.47, 21.77, 13.88. HPLC Rt: 2.303, LC/MS calculated for expected $C_{18}H_{26}BrN_3O_4$ [M]: 428.32; found: [M][+]: 428, [M + 2][+]: 430; anal. calcd for $C_{18}H_{26}BrN_3O_4$ (exact mass: 427.11; MW: 428.32): C, 50.47; H, 6.12; N, 9.81; O, 14.94; found: C, 50.56; H, 6.33; N, 9.70; O, 14.90% (^{1}H NMR, ^{13}C NMR, and mass spectra of compound **7a** are shown in the ESI,† Fig. S1–S3 respectively).

N^1-Butyl-2-(2-(2-fluorophenyl)acetamido)-N^5-hydroxypentanediamide (7b). Yield 57.46%, white powder, ^{1}H NMR (400 MHz, DMSO-d_6) δ 10.43 (s, 1H), 8.71 (s, 1H), 8.29 (d, J = 8.1 Hz, 1H), 7.92 (t, J = 5.8 Hz, 1H), 7.34–7.24 (m, 2H), 7.16–7.10 (m, 2H), 4.24 (td, J = 8.2, 5.7 Hz, 1H), 3.55 (s, 2H), 2.96–2.80 (m, 2H), 2.01–1.61 (m, 5H), 0.82 (d, J = 6.7 Hz, 6H). ^{13}C NMR (101 MHz, DMSO-d_6) δ 170.93, 169.00, 168.49, 161.75, 159.32, 131.66, 128.52, 124.09, 115.01, 52.39, 45.91, 34.96, 28.84, 28.51, 27.96, 20.00 HPLC Rt: 2.361 LC/MS calculated for [M]: 353.39; Found: [M + H][+]: 354; anal. calcd for $C_{17}H_{24}FN_3O_4$ (exact mass: 353.18; MW: 353.39): C, 57.78; H, 6.85; N, 11.89; O, 18.11; found: C, 57. 81; H, 6.66; N, 12.1; O, 18.12% (^{1}H NMR, ^{13}C NMR and mass spectra of compound **7b** are shown in the ESI,† Fig. S4–S6 respectively).

2-(2-(4-Bromophenyl)acetamido)-N^5-hydroxy-N^1-pentylpentanediamide (7c). Yield 48%, cream color solid, ^{1}H NMR (400 MHz, DMSO-d_6) δ 8.29 (d, J = 8.1 Hz, 1H), 7.90 (t, J = 5.5 Hz, 1H), 7.47 (d, J = 8.4 Hz, 2H), 7.22 (d, J = 8.4 Hz, 2H), 4.17 (dd, J =

14.9, 6.9 Hz, 1H), 3.50–3.41 (m, 2H), 3.02 (m, 2H), 1.98–1.66 (m, 4H), 1.36 (m, 2H), 1.29–1.17 (m, 5H), 0.84 (t, J = 7.1 Hz, 3H), ^{13}C NMR (101 MHz, DMSO-d_6) δ 171.26, 170.10, 168.93, 136.33, 131.78, 131.46, 119.96, 52.79, 41.71, 38.88, 29.32, 29.10, 28.94, 22.25, 14.36. HPLC Rt: 2.474 LC/MS calculated for expected $C_{18}H_{26}BrN_3O_4$ [M]: 428.32; found: [M][+]: 428, [M + 2][+]: 430, [M + Na][+]: 452; anal. calcd for $C_{18}H_{26}BrN_3O_4$ (exact mass: 427.11; MW: 428.32): C, 50.47; H, 6.12; N, 9.81; O, 14.94; found: C, 50.68; H, 6.08; N, 9.73; O, 14.67% (spectra of compound **7c** are shown in the ESI,† Fig. S7–S9 respectively).

2-(2-(4-Bromophenyl)acetamido)-N^1-hexyl-N^5-hydroxypentanediamide (7d). Yield 92.7%, cream powder, ^{1}H NMR (400 MHz, DMSO-d_6) δ 10.41 (s, 1H), 8.29 (t, J = 8.5 Hz, 1H), 7.91 (t, J = 5.5 Hz, 1H), 7.47 (d, J = 8.4 Hz, 2H), 7.22 (d, J = 8.3 Hz, 2H), 4.17 (dd, J = 14.0, 8.2 Hz, 1H), 3.46 (s, 2H), 3.09–2.95 (m, 2H), 2.20–1.66 (m, 4H), 1.34 (dd, J = 13.2, 6.5 Hz, 2H), 1.23 (d, J = 4.6 Hz, 6H), 0.85 (dd, J = 8.5, 5.0 Hz, 3H), ^{13}C NMR (101 MHz, DMSO-d_6) δ 170.75, 169.57, 168.43, 135.84, 131.28, 130.95, 119.45, 52.30, 41.20, 38.40, 30.90, 28.90, 28.84, 28.45, 25.91, 22.00, 13.88. HPLC Rt: 2.447 LC/MS calculated for expected $C_{19}H_{28}BrN_3O_4$ [M]: 442.35; Found: [M][+]: 442, [M + 2][+]: 444; anal. calcd for $C_{19}H_{28}BrN_3O_4$ (exact mass: 441.13; MW: 442.35): C, 51.59; H, 6.38; N, 9.50; O, 14.47; found: C, 51.78; H, 6.23; N, 9.79; O, 14.1% (^{1}H NMR, ^{13}C NMR and mass spectra of compound **7d** are shown in the ESI,† Fig. S10–S12 respectively).

N^1-Butyl-2-(2-(4-chlorophenyl)acetamido)-N^5-hydroxypentanediamide (7e). Yield 60%, cream color solid, ^{1}H NMR (400 MHz, DMSO-d_6) δ 10.39 (s, 1H), 8.26 (d, J = 8.1 Hz, 1H), 7.88 (t, J = 5.6 Hz, 1H), 7.38–7.33 (m, 2H), 7.28 (d, J = 8.5 Hz, 2H), 4.22–4.12 (m, 1H), 3.48 (s, 1H), 3.03 (m, 1H), 1.97–1.60 (m, 2H), 1.40–1.17 (m, 7H), 0.86 (m, 3H). ^{13}C NMR (101 MHz, DMSO-d_6) δ 171.25,

170.15, 168.91, 167.46, 135.91, 132.18, 132.06, 131.49, 131.38, 131.25, 129.13, 128.54, 67.87, 52.77, 41.65, 38.58, 31.56, 30.26, 29.48, 29.30, 28.95, 28.83, 23.71, 22.86, 19.92, 14.36, 14.11, 11.27. HPLC Rt: 2.955 LC/MS calculated for expected $C_{17}H_{24}ClN_3O_4$ [M]: 369.84; Found: $[M + H]^+$: 370, $[M + Na]^+$: 392; anal. calcd for $C_{17}H_{24}ClN_3O_4$ (exact mass: 369.15; MW: 369.84): C, 55.21; H, 6.54; N, 11.36; O, 17.30; found: C, 56.09; H, 6.23; N, 11.42; O, 16.83% (^{1}H NMR, ^{13}C NMR, and mass spectra of compound **7e** are shown in the ESI,† Fig. S13–S15 respectively).

2-(2-(4-Chlorophenyl)acetamido)-N^5-hydroxy-N^1-pentylpenta-nediamide (7f). Yield 80%, white crystals, ^{1}H NMR (400 MHz, DMSO-d$_6$) δ 8.31 (d, J = 8.1 Hz, 1H), 7.92 (t, J = 5.4 Hz, 1H), 7.34 (d, J = 8.4 Hz, 2H), 7.28 (d, J = 8.4 Hz, 2H), 4.18 (dd, J = 13.7, 7.9 Hz, 1H), 3.48 (s, 2H), 3.02 (m, 2H), 1.98–1.67 (m, 4H), 1.41–1.32 (m, 2H), 1.24 (m, 5H), 0.84 (t, J = 7.0 Hz, 3H). ^{13}C NMR (101 MHz, DMSO-d$_6$) δ 171.28, 170.19, 168.94, 135.90, 131.50, 131.38, 128.53, 52.81, 29.32, 29.10, 28.94, 22.24, 14.35. HPLC Rt: 2.362, LC/MS calculated for expected $C_{18}H_{26}ClN_3O_4$ [M]: 383.87; $[M + H]^+$: 384, $[M + Na]^+$: 406; anal. calcd for $C_{18}H_{26}ClN_3O_4$ (exact mass: 383.16; MW: 383.87): C, 56.32; H, 6.83; N, 10.95; O, 16.67; found: C, 56.13; H, 6.7; N, 11.3; O, 16.27% (^{1}H NMR, ^{13}C NMR, and mass spectra of compound **7f** are shown in the ESI,† Fig. S16–S18 respectively).

N^1-Butyl-N^5-hydroxy-2-(2-(4-nitrophenyl)acetamido)pentane-diamide (7g). Yield 57.9%, pale yellow powder, ^{1}H NMR (400 MHz, DMSO-d$_6$) δ 8.44 (d, J = 8.1 Hz, 1H), 8.17 (d, J = 8.7 Hz, 2H), 7.95 (t, J = 5.5 Hz, 1H), 7.54 (d, J = 8.8 Hz, 2H), 4.19 (dd, J = 13.8, 8.2 Hz, 1H), 3.67 (s, 2H), 3.04 (m, 2H), 1.98–1.67 (m, 3H), 1.39–1.19 (m, 5H), 0.87–0.82 (m, 3H), ^{13}C NMR (101 MHz, DMSO-d$_6$) δ 170.69, 168.89, 168.41, 146.18, 144.55, 130.37, 123.22, 52.39, 41.61, 38.09, 31.06, 28.81, 28.46, 19.42, 13.60. HPLC Rt: 3.388, LC/MS calculated for expected $C_{17}H_{24}N_4O_6$ [M]: 380.40; $[M + H]^+$: 381, $[M + Na]^+$: 403; anal. calcd for $C_{17}H_{24}N_4O_4$ (exact mass: 383.16; MW: 383.87): C, 53.68; H, 6.36; N, 14.73; O, 25.24; found: C, 53.69; H, 6.4; N, 14.98; O, 24.99% (^{1}H NMR, ^{13}C NMR, and mass spectra of compound **7g** are shown in the ESI,† Fig. S19–S21 respectively).

N^1-Butyl-2-(2-(2,4-dichlorophenyl)acetamido)-N^5-hydroxypenta-nediamide (7h). Yield 92%, cream powder, ^{1}H NMR (400 MHz, DMSO-d$_6$) δ 8.29 (d, J = 8.1 Hz, 1H), 7.90 (t, J = 5.6 Hz, 1H), 7.57 (s, 1H), 7.38 (s, 2H), 4.21 (m, 1H), 3.65 (d, J = 3.0 Hz, 2H), 3.11–2.99 (m, 2H), 2.01–1.69 (m, 3H), 1.41–1.21 (m, 5H), 0.86 (t, J = 7.3 Hz, 3H), ^{13}C NMR (101 MHz, DMSO-d$_6$) δ 173.81, 170.69, 168.46, 134.53, 133.53, 133.13, 131.91, 128.34, 127.04, 52.34, 38.09, 31.08, 30.10, 28.82, 28.45, 19.43, 13.62. HPLC Rt: 2.526, LC/MS calculated for expected $C_{17}H_{23}Cl_2N_3O_4$ [M]: 404.29; $[M]^+$: 404, $[M + 2]$: 406; anal. calcd for $C_{17}H_{23}Cl_2N_3O_4$ (exact mass: 403.11; MW: 404.29): C, 50.50; H, 5.73; N, 10.39; O, 15.83; found: C, 50.68; H, 6.07; N, 10.64; O, 15.13% (^{1}H NMR, ^{13}C NMR, and mass spectra of compound **7h** are shown in the ESI,† Fig. S22–S24 respectively).

2-(2-(2,4-Dichlorophenyl)acetamido)-N^5-hydroxy-N^1-pentyl-pentanediamide (7i). Yield 88.6%, white powder, ^{1}H NMR (400 MHz, DMSO-d$_6$) δ 8.72 (s, 1H), 8.66 (d, J = 8.1 Hz, 1H), 7.91 (t, J = 5.6 Hz, 1H), 7.68 (s, 1H), 7.50 (d, J = 0.9 Hz, 2H), 4.34 (m, 1H), 3.14–3.01 (m, 2H), 2.12–1.75 (m, 4H), 1.39 (dd, J = 13.1, 6.4 Hz, 2H), 1.31–1.15 (m, 6H), 0.86 (t, J = 6.7 Hz, 3H), ^{13}C NMR

(101 MHz, DMSO-d$_6$) δ 170.36, 168.44, 165.29, 135.30, 134.49, 131.23, 130.51, 129.02, 127.11, 52.93, 38.49, 30.93, 28.95, 28.91, 27.96, 25.93, 22.02, 13.88. HPLC Rt: 2.810, LC/MS calculated for expected $C_{18}H_{25}Cl_2N_3O_4$ [M]: 418.31; $[M]^+$: 418, $[M + 2]^+$: 420; anal. calcd for $C_{18}H_{25}Cl_2N_3O_4$ (exact mass: 417.12; MW: 418.31): C, 51.68; H, 6.02; N, 10.05; O, 15.30; found: C, 51.73; H, 5.99; N, 10.02; O, 15.49% (^{1}H NMR, ^{13}C NMR, and mass spectra of compound **7i** are shown in the ESI,† Fig. S25–S27 respectively).

2-(2-(2,4-Dichlorophenyl)acetamido)-N^5-hydroxy-N^1-phenyl-pentanediamide (7j). Yield 40%, off white powder, ^{1}H NMR (400 MHz, DMSO-d$_6$) δ 8.75 (t, J = 9.0 Hz, 1H), 8.48 (t, J = 5.8 Hz, 1H), 7.68 (d, J = 1.2 Hz, 1H), 7.55–7.48 (m, 2H), 7.35–7.21 (m, 5H), 4.42 (m, 1H), 4.32 (d, J = 5.8 Hz, 2H), 2.15–1.95 (m, 3H), 1.91–1.80 (m, 1H), ^{13}C NMR (101 MHz, DMSO-d$_6$) δ 170.74, 170.72, 168.43, 165.45, 139.27, 139.23, 135.24, 134.53, 131.28, 130.56, 129.03, 128.23, 127.11, 127.04, 126.74, 53.06, 42.07, 28.94, 27.79. HPLC Rt: 2.712 LC/MS calculated for expected $C_{19}H_{19}Cl_2N_3O_4$ [M]: 424.28; $[M]^+$: 424, $[M + 2]^+$: 426; anal. calcd for $C_{19}H_{19}Cl_2N_3O_4$ (exact mass: 423.08; MW: 424.28): C, 53.79; H, 4.51; N, 9.90; O, 15.08; found: C, 53.71; H, 4.80; N, 9.89; O, 14.98% (^{1}H NMR, ^{13}C NMR, and mass spectra of compound **7j** are shown in the ESI,† Fig. S28–S30 respectively).

N^5-Hydroxy-N^1-pentyl-2-(2-phenylacetamido)pentanediamide (7k). Yield 95.2%, white powder, ^{1}H NMR (400 MHz, DMSO-d$_6$) δ 8.39 (d, J = 8.2 Hz, 1H), 8.11–8.06 (m, 1H), 7.91 (m, 2H), 7.84–7.78 (m, 1H), 7.54–7.40 (m, 4H), 4.22 (m, 1H), 3.97 (d, J = 4.1 Hz, 1H), 3.09–2.95 (m, 2H), 2.01–1.69 (m, 4H), 1.41–1.15 (m, 7H), 0.84 (t, J = 7.1 Hz, 3H), ^{13}C NMR (101 MHz, DMSO-d$_6$) δ 170.79, 169.96, 168.48, 133.28, 132.80, 131.95, 128.28, 127.70, 126.96, 125.85, 125.56, 125.43, 124.29, 52.31, 38.39, 28.87, 28.61, 28.52, 28.45, 21.74, 13.85. HPLC Rt: 2.359, LC/MS calculated for expected $C_{22}H_{29}N_3O_4$ [M]: 399.48; $[M + H]^+$: 400, $[M + Na]^+$: 422; anal. calcd for $C_{22}H_{29}N_3O_4$ (exact mass: 399.22; MW: 399.48): C, 66.14; H, 7.32; N, 10.52; O, 16.02; found: C, 66.13; H, 7.51; N, 10.39; O, 16.25% (^{1}H NMR, ^{13}C NMR, and mass spectra of compound **7k** are shown in the ESI,† Fig. S31–S33 respectively).

N^1-Hexyl-N^5-hydroxy-2-(2-phenylacetamido)pentanediamide (7l). Yield = 76.2%, white crystalline powder, ^{1}H NMR (400 MHz, DMSO-d$_6$) δ 10.43 (s, 1H), 8.42 (d, J = 8.1 Hz, 1H), 8.12–8.05 (m, 1H), 7.93–7.87 (m, 2H), 7.81 (dd, J = 6.3, 3.0 Hz, 1H), 7.53–7.41 (m, 4H), 4.24–4.17 (m, 1H), 3.98 (d, J = 2.8 Hz, 2H), 3.07–2.96 (m, 2H), 2.03–1.68 (m, 5H), 1.39–1.18 (m, 9H), 0.85 (t, J = 6.7 Hz, 3H). ^{13}C NMR (101 MHz, DMSO-d$_6$) δ 171.32, 170.49, 169.02, 133.77, 133.31, 132.45, 128.78, 128.22, 127.46, 126.35, 126.06, 125.93, 124.81, 52.87, 31.39, 29.40, 29.01, 26.30, 22.48, 21.54, 14.37. LC-MS calculated for expected $C_{23}H_{31}N_3O_4$ [M]: 413.51 and found $[M + H]^+$: 414; anal. calcd for $C_{23}H_{31}N_3O_4$ (exact mass: 413.23; MW: 413.51): C, 66.81; H, 7.56; N, 10.16; O, 15.48; found: C, 66.59; H, 7.67; N, 10.07; O, 15.67% (^{1}H NMR, ^{13}C NMR, and mass spectra of compound **7l** are shown in the ESI,† Fig. S34–S36 respectively).

HDAC inhibition assay and selectivity of compounds

All target compounds were screened for their HDAC enzyme inhibition efficiency.[16] First, we tested these compounds on
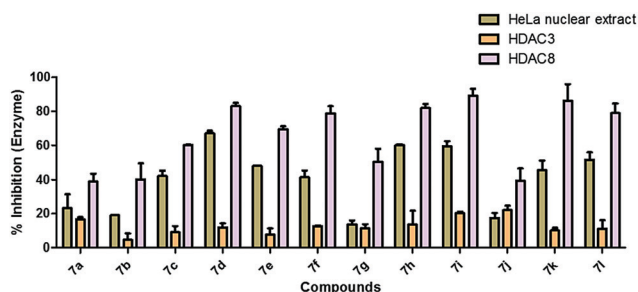
Fig. 4 HDAC inhibition efficiency of all target compounds. All novel compounds were screened at 10 μM concentration on HeLa nuclear extract, human recombinant HDAC3, and human recombinant HDAC8.

Fig. 5 Dose response curves of **7d**, **7e**, **7f**, **7h**, **7i**, **7k**, **7l**, and SAHA in HDAC8 inhibition assay [the data represents mean ± SD (n = 3)].

HeLa nuclear extract, which is rich in HDAC1 and HDAC2 enzymes.[36] It was observed that compounds **7c**, **7d**, **7e**, **7f**, **7h**, **7i**, **7k**, and **7l** were showing good inhibition (Fig. 4 and Table 4).

Again, they were tested on human recombinant HDAC8 at the same concentration (10 μM). Almost all compounds were found to show promising HDAC8 inhibition. Particularly, compounds **7d**, **7f**, **7h**, **7i**, **7k**, and **7l** were showing more than 80% HDAC8 inhibition. Another Class I HDAC, HDAC3 was also screened for inhibition by these compounds. These compounds were found to show minimal inhibition of HDAC3. These results demonstrate the selectivity of these compounds towards the HDAC8 enzyme. More interestingly, these results are in agreement with the prediction results from the MLR and SVM models, as demonstrated in Table 4.

Regarding the HDAC enzyme inhibition, it was noticed that a number of compounds (compounds **7c–7h**, **7i**, **7k**, and **7l**) showed effective HDAC8 inhibition (>50% at 10 μM). Among these, compounds **7f**, **7g**, and **7k** exhibited HDAC8 selectivity over HeLa nuclear extract and HDAC3/NCoR1. On the other hand, the other compounds are not very HDAC8 selective (Fig. 5).
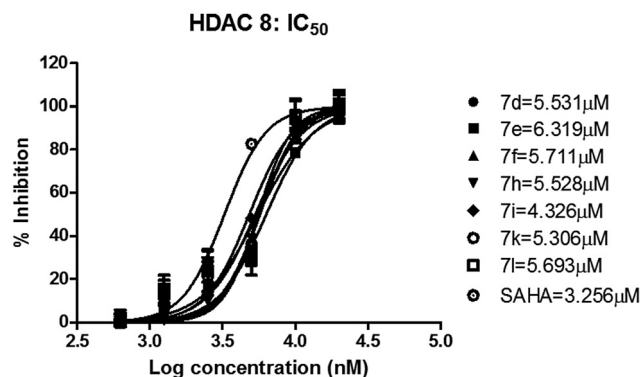
Cell culture studies using anticancer cell lines

Antiproliferative assay using cancer cell lines (MTT assay). Cytotoxicity studies were performed on three different cell lines, *i.e.*, B16F10 (murine melanoma cell line), non-small cell lung cancer cell line (A549), and human acute T cell lymphoblastic leukemia (Jurkat E6.1) by MTT assay method. These synthesized compounds were evaluated at two different concentrations (100 and 10 μM) in triplicate (Fig. 6A–C).

From the assay results, it was observed that few compounds displayed good cytotoxicity with a similar trend on these cell lines. Promising compounds (**7d**, **7e**, **7f**, **7h**, **7i**) were further screened to find out their IC$_{50}$ values in all three cell lines. Results are displayed in Fig. S37A–C in ESI† and Table 5.

Increased activity was observed with compounds having an alkyl side chain with five carbon atoms. This length is the most suitable as four and six carbon chains showed comparatively lesser activity. Again, substitution on the phenyl ring showed an impact on the activity. It was interesting to note that

Table 4 %HDAC inhibition of target compounds in HeLa nuclear extract, human recombinant HDAC3, and human recombinant HDAC8

Comp[a]	R[1]	R[2]	% Inhibition at 10 μM			Observed HDAC8/HDAC3 selectivity range[b]	Average predicted HDAC8/ HDAC3 selectivity range[c]
			HeLa nuclear extract	HDAC3/NCoR1	HDAC8		
7a	2-Br	n-C$_5$H$_{11}$	23.25	16.71	38.84	SEL	SEL
7b	2-F	i-C$_4$H$_9$	19.14	4.65	40.17	SEL	SEL
7c	4-Br	n-C$_5$H$_{11}$	42.24	9.02	60.24	SEL	SEL
7d	4-Br	n-C$_6$H$_{13}$	67.16	11.96	83.14	SEL	SEL
7e	4-Cl	n-C$_4$H$_9$	48.12	7.73	69.66	SEL	SEL
7f	4-Cl	n-C$_5$H$_{11}$	41.46	12.67	78.84	SEL	SEL
7g	4-NO$_2$	n-C$_4$H$_9$	13.77	11.36	50.61	SEL	SEL
7h	2,4-Dichloro	n-C$_4$H$_9$	60.11	13.63	82.05	SEL	SEL
7i	2,4-Dichloro	n-C$_5$H$_{11}$	59.42	20.33	89.17	SEL	SEL
7j	2,4-Dichloro	C$_6$H$_5$	17.43	22.11	39.44	SEL	SEL
7k	—	n-C$_5$H$_{11}$	45.52	10.10	86.38	SEL	SEL
7l	—	n-C$_6$H$_{13}$	51.69	11.08	78.94	SEL	SEL

[a] Compound number. [b] Observed selectivity (negative logarithmic ratio of HDAC8/HDAC3). [c] Average predicted selectivity as per the QAAR models shown for comparison; SEL, HDAC8 selective.
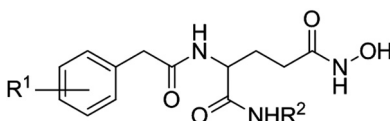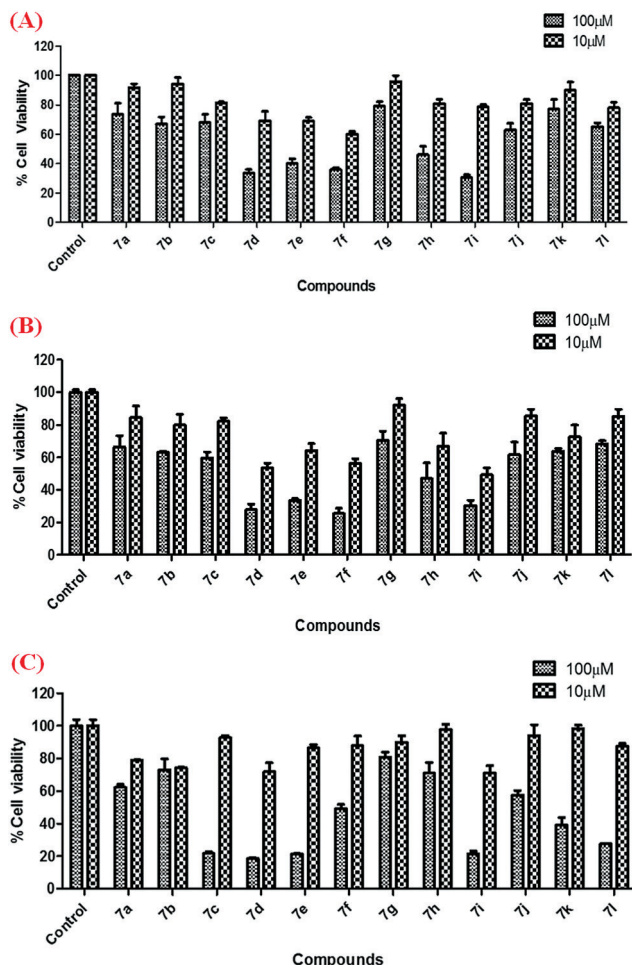
Fig. 6 MTT assay of the synthesized compounds on (A) B16F10, (B) A549, and (C) Jurkat E6.1 cell lines. Cells were treated for 72 h, and cell viability was measured by MTT reagent. Data represent mean ± SD (n = 3).

compounds with bulky halogen substitution at the R^1 position (compounds **7d–7f**, **7h**, **7i**) display cytotoxicity in the cancer cell lines tested. Apart from that, the *n*-pentyl substitution at the R^2 position (compounds **7f**, **7i**) was found to be optimum compared to the *n*-butyl (compounds **7e**, **7h**) and *n*-hexyl substitution (compound **7d**). Importantly, aryl substitution (such as phenyl) at the R^2 position yielded inactivity (compound **7j**). Again, naphthylacetyl derivatives (compounds **7k**, **7l**) were found to be ineffective.

Cell cycle analysis

We further investigated the effect of compounds **7f** and **7i** on cell cycle progression in the representative cancer B16F10 cell line (Fig. 7).

From the result, it was found that compounds **7f** and **7i** induced growth arrest at the G2/M phase of cell growth. Compound **7i** induced significant growth arrest around 42.8% in the G2/M phase compared to control, showing 9.32%, while G0/G1 phase decreased to 10.5% from 74.6%. A similar pattern of growth arrest was found for **7f** also. These results indicated that

Table 5 IC$_{50}$ values of target compounds in different cancer cell lines

Comp[a]	R^1	R^2	IC$_{50}$ (μM) inB16F10 cell line	IC$_{50}$ (μM) in A549 cell line	IC$_{50}$ (μM) in Jurkat E6.1 cell line
7a	2-Br	*n*-C$_5$H$_{11}$	> 50	> 50	> 50
7b	2-F	i-C$_4$H$_9$	> 50	> 50	> 50
7c	4-Br	*n*-C$_5$H$_{11}$	> 50	> 50	> 50
7d	4-Br	*n*-C$_6$H$_{13}$	34.71	31.47	28.66
7e	4-Cl	*n*-C$_4$H$_9$	38.16	38.03	34.42
7f	**4-Cl**	***n*-C$_5$H$_{11}$**	27.72	20.33	18.57
7g	4-NO$_2$	*n*-C$_4$H$_9$	> 50	> 50	> 50
7h	2,4-Dichloro	*n*-C$_4$H$_9$	32.21	33.39	30.08
7i	**2,4-Dichloro**	***n*-C$_5$H$_{11}$**	28.13	22.54	17.24
7j	2,4-Dichloro	C$_6$H$_5$	> 50	> 50	> 50
7k	—	*n*-C$_5$H$_{11}$	> 50	> 50	> 50
7l	—	*n*-C$_6$H$_{13}$	> 50	> 50	> 50

[a] Compound number.

compound **7i** may produce anticancer activity with the growth arrest at the G2/M phase (Fig. 7).

Binding mode of interaction study

Since we earlier performed the binding mode of interaction studies of carboxylic acid derivatives,[8] we tried the same for hydroxamate derivatives here. The molecular docking study[37] revealed that all these compounds were almost superimposed in the active site of HDAC8 (PDB: 1VKG) (Fig. 8). The hydroxamate moiety of these compounds closely resided with the Zn^{2+} ion (Fig. 8).

The molecular docking interaction of the two prototype compounds (**7i** and **7f**) showed that the carbonyl group of the hydroxamate moiety had an interaction with the Zn^{2+} ion (Fig. 9). Again, the carbonyl group of the hydroxamate moiety accepts a hydrogen bond from Tyr306.

Moreover, Tyr306 at the active site accepts hydrogen bonds from the amide group attached with the *n*-pentyl moiety. The 4-chlorobenzyl group formed two π–π stacking interactions with Phe152 and Phe208. Notably, two parallel-displayed π–π interactions (F192 and F208) are also important signs for good HDAC8 interaction.[38] In the case of compound **7f**, Tyr306 amino acid residue accepts hydrogen bonds from the amide group attached with the *n*-pentyl moiety. Tyr306 also donates hydrogen bond to the carbonyl function of the hydroxamate moiety. Interaction of these targeted compounds with Y306 (which is not present in HDAC4)[39] could be the reason for the observed HDAC8 selectivity. Interestingly, the molecular docking study of these compounds against other HDACs was not so encouraging.

Conclusion

This study presents the first QAAR model for investigating structural requirements to attain HDAC8 selectivity over HDAC3. Robust QSAR models were evolved from the linear and non-linear techniques and were validated by means of internal and external validation tests. The developed QAAR models were utilized to design new molecules having HDAC8 selectivity. Then, design compounds were synthesized and characterized. All target compounds were evaluated for their
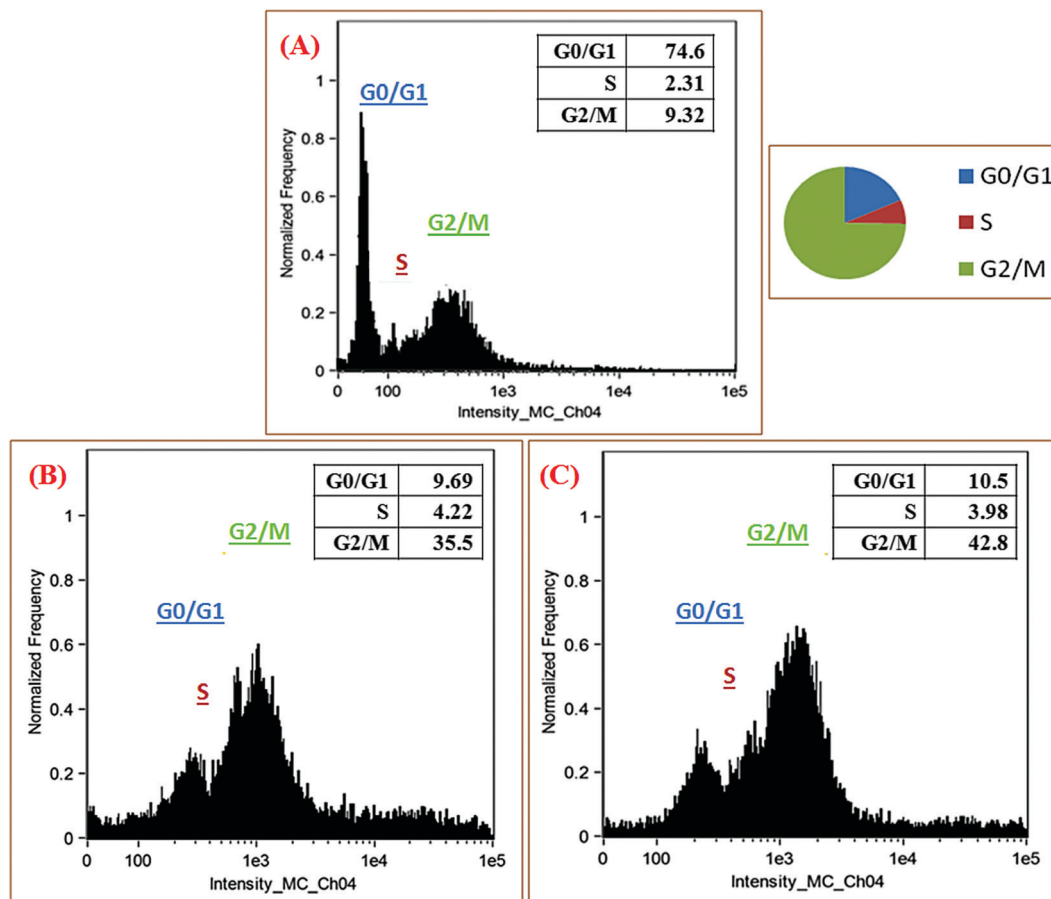
Fig. 7   Cell cycle arrest induced in B16F10 cell line by (A) control, (B) **7f**, (C) **7i**.
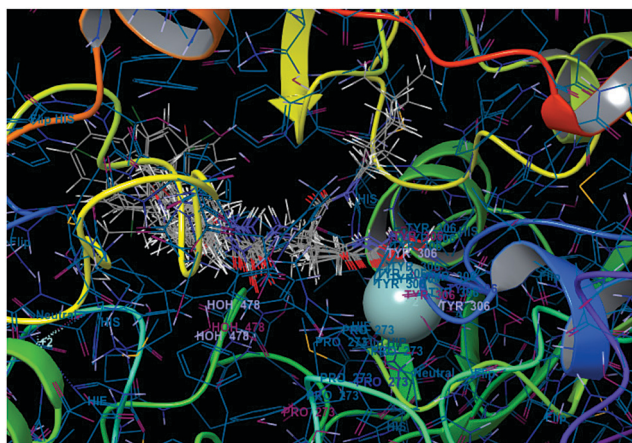

Fig. 8   The docked conformations of compounds (grey lines) superimposed with each other at the active site of HDAC8 (PDB: 1VKG).

HDAC enzyme inhibition efficiency with HeLa nuclear extract, human recombinant HDAC3, and human recombinant HDAC8 enzymes. Interestingly, these compounds were found to be effective HDAC inhibitors with preferential selectivity for HDAC8. The five-carbon side chain was found to be the most appropriate length for the linker moiety.

These compounds were also tested for their antiproliferative activity in three different cell lines (B16F10, HeLa, and Jurkat E6.1) for murine melanoma, non-small cell lung carcinoma (NSCLC), and acute lymphoblastic leukemia (ALL) types of cancer. Promising compounds were also explored for their IC$_{50}$ calculation in these cell lines. Compounds **7f** and **7i** were found to possess efficient anticancer potential in MTT assay. Compound **7f** and **7i** induced significant cell growth arrest in the G2/M phase, indicating good anticancer potential in cell cycle analysis of representative cancer murine melanoma B16F10 cell line. These compounds (**7f** and **7i**) showed a binding mode of interactions with the HDAC8 enzyme.

Notably, these compounds can be further modified to improve their efficacy and selectivity. Likewise, one has to consider the requisite structural features from the QAAR models and then can predict the selectivity values using reported QAAR models. Further, the developed models can be used as efficient query tools for screening selective HDAC8 inhibitors. Together, this study offers an understanding of the essential structural features or properties of the molecules for proper binding in the active site of the HDAC8 enzyme and may help to get better selective HDAC8 inhibitors as anticancer agents in the future.
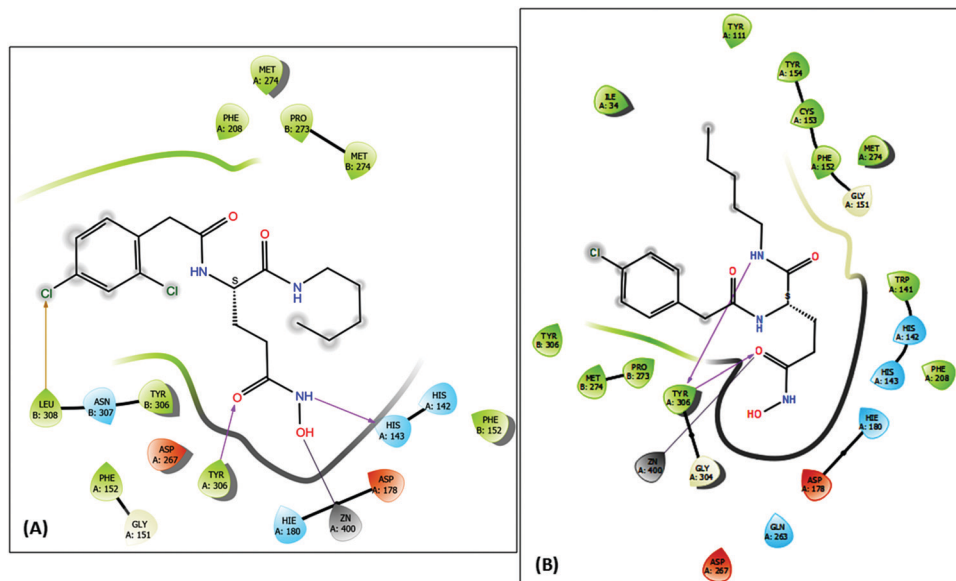
Fig. 9 Molecular docking interactions of (A) compound **7i** and (B) compound **7f** with HDAC8 enzyme (PDB: 1VKG).

Experimental section

Design of molecules: QAAR studies

To achieve robust quantitative activity–activity relationship (QAAR) model, series of investigations, including dataset preparation and descriptor calculations, were performed followed by regression analysis with different multivariate methods.

Data set

A dataset containing fifty-nine diverse molecules having HDAC8 and HDAC3 inhibitory activities was collected from the published work of the University of Illinois at Chicago[17–26] to perform the QAAR studies. These compounds include aliphatic and aromatic hydrocarbons, heteroaromatic, amide, ester, keto, and sulphonyl compounds, as shown in Table S1 of the ESI.†

Descriptor generation

The 2D structures of investigated compounds were drawn by ChemDraw Ultra 8.0 software,[27] and subsequently, the molecular structures were subjected to geometry optimizations. The energy minimizations were carried out by a molecular orbital package (MOPAC) module with 100 iterations, and the minimum RMS gradient was 0.10. Then, the 2D descriptors were calculated from the freely available software "PaDEL-descriptor".[28] Initially, descriptors with constant values, which did not cover the whole space, were deleted from the study to decrease the redundancy.[11]

Multivariate regression analysis

Multivariate regression was performed to correlate the independent descriptors, which in our case are the "PaDEL-descriptors", with the dependent variable ($pIC_{50}^{HDAC8/HDAC3}$).

Two supervised learning approaches, namely multiple linear regression (MLR) and support vector machine (SVM) were used.[29,30]

MLR based 2D-QAAR study was employed here to correlate molecular descriptors with biological activity. The predictability of the developed stepwise multiple linear regression (S-MLR) model was evaluated using both internal and external validation matrices.[11,31–33]

For the construction of the SVM model, we used John Platt's Sequential Minimal Optimization (SMO) algorithm with the Waikato Environment for Knowledge Analysis (Weka) version 3.8.4.[34–36] SVM is a learning approach based on the statistical learning theory. Recently, this technique received huge success in modeling biological and chemical properties. Here, the SVM parameters (The complexity parameter C = 1.0, exponent E = 1.0, epsilon parameter = 0.001, tolerance T = 0.001) were used to construct the SVM model.[11]

Chemistry

All starting materials and reagents were commercially available and used without further purification. All reactions were monitored by thin layer chromatography (TLC) using precoated plates with silica gel F254 from Merck Millipore Co., USA. ^{1}H and ^{13}C NMR spectra were recorded in DMSO-d$_6$ using Nuclear Magnetic Resonance (NMR) Spectrophotometer High Performance-400 MHz (Bruker Biospin, Switzerland). Mass spectroscopy was performed in LCMS-2020, Shimadzu using ESI mode. The purity of these compounds was analyzed by analytical LC/MS. Analysis was performed on an LCMS-8040 equipped with a photodiode array detector using a Shiseido C18 4.6 × 150 mm, 5μ column at a flow rate of 1 mL/min with the isocratic flow (20% A: 80% B; solvent A = water + 0.4% TFA, solvent B = methanol).

Synthesis of substituted pentanoic acid derivatives (6a–6l)

The substituted pentanoic acids (5a–5l) were dissolved in anhydrous methanol and the flask was kept in an ice bath to get 0 °C temperature (Scheme 1). Thionyl chloride (1.5–2 ml) was added dropwise to the above mixture and stirred overnight. The reaction mixture was concentrated and extracted with ethyl acetate. The organic layer was washed individually with aqueous saturated sodium bicarbonate and brine solutions separately. The crude organic mixture was purified individually by column chromatography using EtOAc : hexane (3 : 7) as the mobile phase.

Synthesis of substituted hydroxamic acid (7a–7l)

The intermediate substituted esters (6a–6l) were dissolved in methanol separately. 50% w/v aqueous hydroxylamine (18.5 equivalents) was added individually to it and stirred for 30 min at room temperature. To the above mixture, sodium hydroxide (1 M, 2 equivalents) solution was added and stirred for 1.5 h separately. The reaction mixture was concentrated and poured in ice cold water individually. It was neutralized by 1 M hydrochloric acid separately. The product was extracted with ethyl acetate, dried over anhydrous sodium sulphate, and evaporated to get the final product (7a–7l).

HDAC inhibition assay

HeLa nuclear extract assay. The HDAC enzyme inhibition assay was performed as mentioned in our earlier publications by using HDAC colorimetric assay kit (BML-AK501, ENZO life sciences) following vendor's protocol. Briefly, 5 μL of HeLa nuclear extract (BML-KI137-0500), 10 μL of assay buffer (BML-KI143-0020), and 10 μL of sample solution were added per well in a microtiter plate. 25 μL of *Color de Lys*® substrate (BML-KI138-0050) was added, and the plate was incubated in an incubator for 30 min at 37 °C, which was terminated by the addition of a 50 μL mixture of developer plus stop solution. The plate was incubated for 15 min at 37 °C, and absorbance was measured at 405 nm. All synthesized compounds were screened at 10 μM concentration in triplicate.

HDAC3/NCOR1 assay. HDAC3 enzyme inhibition assay was performed using HDAC3/NCOR1 fluorimetric drug discovery kit (BML-AK531, ENZO life sciences) following vendor's protocol. Here, 10 μL of sample solution and 15 μL diluted HDAC3/NCOR1 complex solution (BML-KI574-0030) were added per well in a microtiter plate. 25 μL Fluor de Lys® substrate solution (BML-KI177-0005) was added. The plate was incubated for 15 min at 37 °C. Then, 50 μL of a mixture of *Fluor de Lys*® developer II (BML-KI176-1250) and trichostatin A (BML-GR309-9090) was added per well and incubated for 45 min at 37 °C. The fluorescence intensity was measured at an excitation wavelength of 360 nm and emission wavelength of 460 nm using Spectramax M4 (Molecular Devices, USA). All synthesized compounds were screened at 10 μM concentration in triplicate.

HDAC8 assay using human recombinant HDAC8. HDAC8 inhibition assay was performed using HDAC8 fluorimetric drug discovery kit (BML-AK518, Enzo life science) following vendor's

protocol. Briefly, 15 μL of diluted human recombinant HDAC8 enzyme (BML-SE145-0100) was incubated with 10 μL of test inhibitor (10 μM), 25 μl of *Fluor de Lys*® HDAC8, and deacetylase substrate (BML-KI178-0005). After 10 min incubation, the reaction was terminated by adding 50 μL stop solution containing *Fluor de Lys*®- Developer II (BML-KI176-1250) and trichostatin A. The plate was incubated for 45 min at 37 °C, and fluorescence intensity was measured by using Spectramax M4 (Molecular Devices, USA). All target compounds were screened at 10 μM concentration in triplicate.

Cell culture study

The murine melanoma cell line (B16F10) was cultured in Dulbecco's Modified Eagle Medium (DMEM) (Himedia Laboratories Pvt. Ltd, Mumbai, India), non-small cell lung cancer cells (A549) in Dulbecco's Modified Eagle Medium/ Nutrient Mixture F-12 Ham (DMEM/F12, 1 : 1 mixture, Himedia Laboratories Pvt. Ltd, Mumbai, India), and Jurkat E6.1 cell line in Roswell Park Memorial Institute-1640 (RPMI-1640, Himedia Laboratories Pvt. Ltd, Mumbai, India), supplemented with 10% heat inactivated fetal bovine serum (Himedia Laboratories Pvt. Ltd., Mumbai, India) and 1% of antibiotic solution (10 000 U penicillin and 10 mg streptomycin per ml, Himedia Laboratories Pvt. Ltd, Mumbai, India). Cells were cultured at 37 °C in a humidified atmosphere with 5% CO_2. Stock solutions of all synthesized compounds were prepared in DMSO at a concentration of 100 mM and stored.

MTT assay

The antiproliferative activity of these synthesized compounds was determined as mentioned in our earlier publications by using an MTT assay. 5×10^4 cells were seeded in 96 well plates and incubated overnight. Cells were treated with synthesized compounds at two concentrations (100 and 10 μM) in triplicates and incubated for 72 h. 50 μL of 5 mg mL^{-1} 3-(4,5-dimethylthiazol-2-yl)-2,5-diphenyltetrazolium bromide (MTT; Himedia Laboratories Pvt. Ltd, Mumbai, India) was added and incubated for 4 h. Then Formazan crystals were dissolved using DMSO and evaluated spectrophotometrically at 570 nm and 650 nm using Spectramax M4 (Molecular Devices, USA).

For the determination of IC$_{50}$ values of promising compounds, same procedure was followed as described above, where five compounds (7d, 7e, 7f, 7h, and 7i) were tested at 10 different concentrations as 400, 200, 100, 50, 25, 12.5, 6.25, 3.125, 1.562, and 0.781 μM.

For Jurkat E6.1 cell line, 2×10^4 cells in 100 μL were seeded in 96 well plates and incubated overnight as mentioned in our earlier publications. Treatment concentrations were the same for both experiments as described above for other cell lines. After 72 h incubation with the test compounds, cells were treated with 22 μL of Prestoblue™ (Invitrogen, Life technologies, United States) reagent. The plate was incubated for 2 h, and fluorescence intensity was measured at the excitation wavelength of 560 nm and emission wavelength of 590 nm using Spectramax M4 (Molecular Devices, USA).

Cell cycle analysis

Briefly, 5×10^5 B16F10 cells were seeded in 6 well plates and incubated overnight at 37 °C. The next day, cells were treated with **7d** and **7i**, respectively, and incubated for 72 h. Cells were trypsinized, centrifuged, washed twice with PBS, fixed with 70% ice-cold ethanol, and stored at −20 °C for 24 h. The cells were centrifuged, washed, and resuspended in 500 μL PBS at pH 7.4 containing RNAse (100 μg mL^{-1}) at room temp for 20 min. Propidium iodide (PI) (50 μg mL^{-1} in PBS) was added to stain cellular DNA and kept in the dark for 30 min. Flow cytometry analysis was performed, and the percentage of cells in each phase of the cell cycle was estimated using the IDEAS Software (version 6.0).

Binding mode interaction study

In order to understand the probable enzyme–ligand binding interactions, molecular docking studies of the synthesized compounds were carried out by the Glide module of Maestro v12.1, Schrödinger Inc. USA.[37] Three-dimensional structure of HDAC8 (PDB code: 1VKG) was downloaded from RSCB Protein Data Bank. It was further processed using "*Protein Preparation Wizard*" in Maestro v12.1. Generating states and refinement steps were performed. It automatically added hydrogen atoms and some essential bonds at the missing sites of the proteins. The further refinement steps included optimization of hydrogen bonded groups and restrained minimization using the default force field OPLS_3e. After the optimization process, receptor grid generation was processed to locate the binding pocket. Then, extra precision (XP) docking studies were achieved, and subsequently, the analyses of the binding were performed. The conformations were ranked on the basis of scores and selected as per their interactions with the enzymes as well as docking scores.

Author contributions

Sk. Abdul Amin: conceptualization, investigation, methodology, validation, data curation, writing – original draft, writing – review & editing. Prakruti Trivedi: methodology, validation, data curation, writing – original draft. Nilanjan Adhikari: validation, data curation, writing – original draft. Routholla Ganesh: methodology, validation, data curation. Dhanya Vijayasarathi: methodology, data curation. Sanjib Das: formal analysis, data curation. Balaram Ghosh: project administration, funding acquisition, writing – review & editing. Tarun Jha: conceptualization, project administration, writing – review & editing, final supervision.

Conflicts of interest

Authors do not have any conflict of interest.

Acknowledgements

References

1 M. M. S. Hamoud, S. Pulya, N. A. Osman, Y. Bobde, A. E. A. Hassan, H. A. Abdel-Fattah, B. Ghosh and A. M. Ghanim, Design, synthesis, and biological evaluation of novel nicotinamide derivatives as potential histone deacetylase-3 inhibitors, *New J. Chem.*, 2020, **44**, 9671, DOI: 10.1039/d0nj01274b.

2 T. C. S. Ho, A. H. Y. Chan and A. Ganesan, Thirty years of HDAC inhibitors: 2020 insight and hindsight, *J. Med. Chem.*, 2020, **63**, 12460–12484, DOI: 10.1021/acs.jmedchem.0c00830.

3 S. A. Amin, N. Adhikari and T. Jha, Diverse classes of HDAC8 inhibitors: In search of molecular fingerprints that regulate activity, *Future Med. Chem.*, 2018, **10**, 1589–1602, DOI: 10.4155/fmc-2018-0005.

4 A. K. Halder, S. Mallick, D. Shikha, A. Saha, K. D. Saha and T. Jha, Design of dual MMP-2/HDAC8 inhibitors by pharmacophore mapping, molecular docking, synthesis and biological activity, *RSC Adv.*, 2015, **5**, 72373–72386, DOI: 10.1039/c5ra12606a.

5 H. Chu, Q.-X. He, J. Wang, Y. Hu, Y.-Q. Wang and Z.-H. Lin, In silico design of novel benzohydroxamate-based compounds as inhibitors of histone deacetylase 6 based on 3D-QSAR, molecular docking, and molecular dynamics simulations, *New J. Chem.*, 2020, **44**, 21201–21210, DOI: 10.1039/D0NJ04704J.

6 A. Chakrabarti, I. Oehme, O. Witt, G. Oliveira, W. Sippl, C. Romier, R. J. Pierce and M. Jung, HDAC8: A multifaceted target for therapeutic interventions, *Trends Pharmacol. Sci.*, 2015, **36**, 481–492, DOI: 10.1016/j.tips.2015.04.013.

7 Y. Asfaha, C. Schrenk, L. A. Alves Avelar, A. Hamacher, M. Pflieger, M. U. Kassack and T. Kurz, Recent advances in class IIa histone deacetylases research, *Bioorg. Med. Chem.*, 2019, **27**, 115087, DOI: 10.1016/j.bmc.2019.115087.

8 S. Dutta, A. K. Halder, N. Adhikari, S. A. Amin, S. Das, A. Saha and T. Jha, Synthesis, anticancer activity, structure-activity relationship and binding mode of interaction

studies of substituted pentanoic acids, *Future Med. Chem.*, 2019, **11**, 1679–1702, DOI: 10.4155/fmc-2018-0361.

9 S. A. Amin, N. Adhikari, T. Jha and S. Gayen, First molecular modeling report on novel arylpyrimidine kynurenine monooxygenase inhibitors through multi-QSAR analysis against Huntington's disease: A proposal to chemists!, *Bioorg. Med. Chem. Lett.*, 2016, **26**, 5712–5718, DOI: 10.1016/j.bmcl.2016.10.058.

10 A. M. Srour, N. S. Ahmed, S. S. Abd El-Karim, M. M. Anwar and S. M. El-Hallouty, Design, synthesis, biological evaluation, QSAR analysis and molecular modelling of new thiazol-benzimidazoles as EGFR inhibitors, *Bioorg. Med. Chem.*, 2020, **28**, 115657, DOI: 10.1016/j.bmc.2020.115657.

11 E. Bourguet, K. Ozdarska, G. Moroy, J. Jeanblanc and M. Naassila, Class I HDAC inhibitors: Potential new epigenetic therapeutics for alcohol use disorder (AUD), *J. Med. Chem.*, 2018, **61**, 1745–1766, DOI: 10.1021/acs.jmedchem.7b00115.

12 O. J. Ingham, R. M. Paranal, W. B. Smith, R. A. Escobar, H. Yueh, T. Snyder, J. A. Porco Jr, J. E. Bradner and A. B. Beeler, Development of a potent and selective HDAC8 inhibitor, *ACS Med. Chem. Lett.*, 2016, **7**, 929–932, DOI: 10.1021/acsmedchemlett.6b00239.

13 N. Adhikari, A. K. Halder, S. Mallick, A. Saha, K. D. Saha and T. Jha, Robust design of some selective matrix metalloproteinase-2 inhibitors over matrix metalloproteinase-9 through in silico/fragment-based lead identification and de novo lead modification: Syntheses and biological assays, *Bioorg. Med. Chem.*, 2016, **24**, 4291–4309, DOI: 10.1016/j.bmc.2016.07.023.

14 A. Mukherjee, N. Adhikari and T. Jha, A pentanoic acid derivative targeting matrix metalloproteinase-2 (MMP-2) induces apoptosis in a chronic myeloid leukemia cell line, *Eur. J. Med. Chem.*, 2017, **141**, 37–50, DOI: 10.1016/j.ejmech.2017.09.052.

15 P. Trivedi, N. Adhikari, S. A. Amin, T. Jha and B. Ghosh, Design, synthesis and biological screening of 2-aminobenzamides as selective HDAC3 inhibitors with promising anticancer effects, *Eur. J. Pharm. Sci.*, 2018, **124**, 165–181, DOI: 10.1016/j.ejps.2018.08.030.

16 P. Trivedi, N. Adhikari, S. A. Amin, Y. Bobde, R. Ganesh, T. Jha and B. Ghosh, Design, synthesis, biological evaluation and molecular docking study of arylcarboxamido piperidine and piperazine-based hydroxamates as potential HDAC8 inhibitors with promising anticancer activity, *Eur, J. Pharm. Sci.*, 2019, **138**, 105046, DOI: 10.1016/j.ejps.2019.105046.

17 A. S. Vaidya, R. Neelarapu, A. Madriaga, H. Bai, E. Mendonca, H. Abdelkarim, R. B. van Breemen, S. Y. Blond and P. A. Petukhov, Novel histone deacetylase 8 ligands without a zinc chelating group: Exploring an 'upside-down' binding pose, *Bioorg. Med. Chem. Lett.*, 2012, **22**, 6621–6627, DOI: 10.1016/j.bmcl.2012.08.104.

18 A. P. Kozikowski, Y. Chen, A. Gaysin, B. Chen, M. A. D'Annibale, C. M. Suto and B. C. Langley, Functional differences in epigenetic modulators-superiority of mercaptoacetamide-based histone deacetylase inhibitors relative to hydroxamates in cortical neuron neuroprotection studies, *J. Med. Chem.*, 2007, **50**, 3054–3061, DOI: 10.1021/jm070178x.

19 J. A. Bergman, K. Woan, P. Perez-Villarroel, A. Villagra, E. M. Sotomayor and A. P. Kozikowski, Selective histone deacetylase 6 inhibitors bearing substituted urea linkers inhibit melanoma cell growth, *J. Med. Chem.*, 2012, **55**, 9891–9899, DOI: 10.1021/jm301098e.

20 A. P. Kozikowski, S. Tapadar, D. N. Luchini, K. H. Kim and D. D. Billadeau, Use of the nitrile oxide cycloaddition (NOC) reaction for molecular probe generation: A new class of enzyme selective histone deacetylase inhibitors (HDACIs) showing picomolar activity at HDAC6, *J. Med. Chem.*, 2008, **51**, 4370–4373, DOI: 10.1021/jm8002894.

21 B. He, S. Velaparthi, G. Pieffet, C. Pennington, A. Mahesh, D. L. Holzle, M. Brunsteiner, R. van Breemen, S. Y. Blond and P. A. Petukhov, Binding ensemble profiling with photo-affinity labeling (BEProFL) approach: Mapping the binding poses of HDAC8 inhibitors, *J. Med. Chem.*, 2009, **52**, 7003–7013, DOI: 10.1021/jm9005077.

22 Y. Chen, M. Lopez-Sanchez, D. N. Savoy, D. D. Billadeau, G. S. Dow and A. P. Kozikowski, A series of potent and selective, triazolylphenyl-based histone deacetylases inhibitors with activity against pancreatic cancer cells and Plasmodium falciparum, *J. Med. Chem.*, 2008, **51**, 3437–3448, DOI: 10.1021/jm701606b.

23 R. He, Y. Chen, Y. Chen, A. V. Ougolkov, J. S. Zhang, D. N. Savoy, D. D. Billadeau and A. P. Kozikowski, Synthesis and biological evaluation of triazol-4-ylphenyl-bearing histone deacetylase inhibitors as anticancer agents, *J. Med. Chem.*, 2010, **53**, 1347–1356, DOI: 10.1021/jm901667k.

24 T. Y. Taha, S. M. Aboukhatwa, R. C. Knopp, N. Ikegaki, H. Abdelkarim, J. Neerasa, Y. Lu, R. Neelarapu, T. W. Hanigan, G. R. J. Thatcher and P. A. Petukhov, Design, synthesis, and biological evaluation of tetrahydro-isoquinoline-based histone deacetylase 8 selective inhibitors, *ACS Med. Chem. Lett.*, 2017, **8**, 824–829, DOI: 10.1021/acsmedchemlett.7b00126.

25 T. Y. Taha, S. M. Aboukhatwa, R. C. Knopp, N. Ikegaki, H. Abdelkarim, J. Neerasa, Y. Lu, R. Neelarapu, T. W. Hanigan, G. R. J. Thatcher and P. A. Petukhov, Correction to design, synthesis, and biological evaluation of tetrahydroisoquinoline-based histone deacetylase 8 selective inhibitors, *ACS Med. Chem. Lett.*, 2019, **10**, 1358, DOI: 10.1021/acsmedchemlett.9b00336.

26 R. Neelarapu, D. L. Holzle, S. Velaparthi, H. Bai, M. Brunsteiner, S. Y. Blond and P. A. Petukhov, Design, synthesis, docking, and biological evaluation of novel diazide-containing isoxazole- and pyrazole-based histone deacetylase probes, *J. Med. Chem.*, 2011, **54**, 4350–4364, DOI: 10.1021/jm2001025.

27 *ChemDraw Ultra 8.0*, Cambridge Soft Corporation, USA, 2015.

28 C. W. Yap, PaDEL-descriptor: An open source software to calculate molecular descriptors and fingerprints, *J. Comput. Chem.*, 2011, **32**, 1466–1474, DOI: 10.1002/jcc.21707.

29 C. Nantasenamat, C. Isarankura-Na-Ayudhya, T. Naenna and V. Prachayasittikul, Prediction of bond dissociation enthalpy of antioxidant phenols by support vector machine,

J. Mol. Graphics Modell., 2008, **27**, 188–196, DOI: 10.1016/j.jmgm.2008.04.005.

30 C. Nantasenamat, A. Worachartcheewan, S. Prachayasittikul, C. Isarankura-Na-Ayudhya and V. Prachayasittikul, QSAR modeling of aromatase inhibitory activity of 1-substituted 1,2,3-triazole analogs of letrozole, *Eur. J. Med. Chem.*, 2013, **69**, 99–114, DOI: 10.1016/j.ejmech.2013.08.015.

31 QSAR tools, DTC laboratory, India; Software available at https://dtclab.webs.com/software-tools (accessed on 23rd March 2021).

32 P. Ambure and K. Roy, Exploring structural requirements of leads for improving activity and selectivity against CDK5/p25 in Alzheimer's disease: An in silico approach, *RSC Adv.*, 2014, **4**, 6702, DOI: 10.1039/c3ra46861e.

33 Organisation for Economic Co-operation and Development, Principles for the validation, for regulatory purposes, of (quantitative) structure–activity relationship models. Available at https://www.oecd.org/chemicalsafety/risk-assessment/37849783.pdf.

34 I. H. Witten and E. Frank, *Data mining: Practical machine learning tools and techniques*, Morgan Kaufmann, San Francisco, 2nd edn, 2005.

35 T. C. Smith and E. Frank, Introducing machine learning concepts with WEKA, *Methods Mol. Biol.*, 2016, **1418**, 353–378, DOI: 10.1007/978-1-4939-3578-9_17.

36 L. A. Serebryannyy, C. M. Cruz and P. de Lanerolle, A role for nuclear actin in HDAC 1 and 2 regulation, *Sci. Rep.*, 2016, **6**, 28460, DOI: 10.1038/srep28460.

37 Schrödinger Suite, 2018. Schrödinger. LLC, New York, USA. http://www.schrodinger.com/glide.

38 M. Morgen, R. R. Steimbach, M. Géraldy, L. Hellweg, P. Sehr, J. Ridinger, O. Witt, I. Oehme, C. J. Herbst-Gervasoni, J. D. Osko, N. J. Porter, D. W. Christianson, N. Gunkel and A. K. Miller, Design and synthesis of dihydroxamic acids as HDAC6/8/10 inhibitors, *ChemMedChem*, 2020, **15**, 1163–1174, DOI: 10.1002/cmdc.202000149.

39 N. Upadhyay, K. Tilekar, N. Jänsch, M. Schweipert, J. D. Hess, L. Henze Macias, P. Mrowka, R. J. Aguilera, J. Y. Choe, F. J. Meyer-Almes and C. S. Ramaa, Discovery of novel N-substituted thiazolidinediones (TZDs) as HDAC8 inhibitors: *in silico* studies, synthesis, and biological evaluation, *Bioorg. Chem.*, 2020, **100**, 103934, DOI: 10.1016/j.bioorg.2020.103934.